

**COMPUTATIONAL APPROACH TO BENDING ACTIVE MODULAR INFLATED SHELLS – STATE OF THE ART**

**S. Gellin<sup>1)</sup>, R. Tarczewski<sup>2)</sup>**

<sup>1)</sup> Buffalo State College, Buffalo NY USA, *SGellin@birdair.com*,

<sup>2)</sup> Wrocław University of Science and Technology, Wrocław Poland, *romuald.tarczewski@pwr.edu.pl*

**ABSTRACT:** A series of papers published by the authors presented theoretical studies to describe the behavior of inflated cushion structures deployed into arched shapes under active bending to span a particular distance. This type of bending active structures is composed of relatively small, modular inflatable cushions combined with cables and cross-braces. The structure is self-erecting. Introduction of tension to the cable gives it shape and load carrying capacity. It was demonstrated that this behavior was equivalent to the classical *elastica* problem. The authors extended this methodology to include the behavior of these structures under a mid-span point load. It was noted that the methodology was limited to deriving shapes that did not include inflection points, and that a modification of the methodology would be required to derive shapes for forces of greater magnitude which would potentially include them. Such a modification was successfully made and the authors noted that the modified methodology used would have greater potential for future studies. In this paper, the authors presents a summary of the results achieved so far, and the resulting conclusions.

**Keywords:** inflatable cushions, active bending, *elastica*, central difference method

**1. INTRODUCTION**

The physical system considered in this paper is a modular inflatable shell. Its structure consists of the three groups of elements: modular inflated cushions (relatively small), tension cables and cross-braces, as shown in Figure 1, top. The latter are optional and are used to increase the structural height. This can also be done by increasing the thickness of the cushions, in the whole structure or part thereof (variable rigidity of the structure). The structure may be shaped as an arc or a single or double curved shell.

The flat structure is assembled at ground level as a near mechanism. It is stabilized and finally shaped in the self-erection process. The essence of the process is the introduction into the structure forces that cause its large deformation (uplift) and give the rigidity. The forces are introduced by pulling the bottom tension cable, thus reducing the distance between the supports. The system becomes bending-active. Figure 1, bottom, shows a general idea of this process.

The structure is assumed to behave elastically, in that a bending stiffness  $EI$  is assumed constant. The authors realize that this is probably not the case; however, the purpose of the theoretical studies is to understand the non-linear behavior due to the bending-thrust interaction without further complication due to non-linear bending stiffness.

This system has been presented previously (see Refs 1-4). The initial experiments confirmed its technological feasibility (Ref. 3). Currently, the authors, in a series of publications (see Refs 5-10, attempted to formulate a calculation model of this type of structures. This paper summarizes the state of the art in this regard, presenting various possible approaches and obtained results.

**2. FORMULATION OF THE CALCULATION MODEL**

Formulation of the calculation model of bending-active inflated shell is a complex problem. The first attempt to computational modeling of modular inflated shell is based on a simplified physical model. The complex internal structure of the shell was approximated by an elastic rod (Ref. 5).

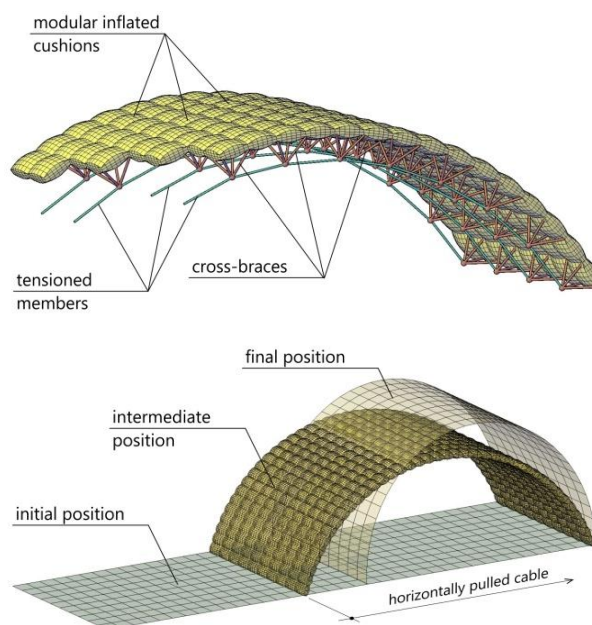


Fig. 1 General composition of modular inflated shell (top) and process of self-erection (bottom)

This allows figuring out the problem from an analytical view point, without being concerned about the details of the construction of the real structure. Issues of determining the flexural stiffness  $EI$  of the structure composed of inflated cushions were omitted. Similarly, were omitted issues of the interaction between the cushions-cross braces system and cable sliding through the nodes of the bottom chord. The adopted methodology has been presented in application to three selected

computational cases. At the end of this paper, information about the ongoing work on formulating the model without the simplifications mentioned above are given.

### 3. APPLICATION OF THE ADOPTED METHODOLOGY TO SELECTED COMPUTATIONAL CASES

Developed methodology has been applied to formulate the calculation model for three cases. The first of these is the self-erection stage, in which the initial shape of the structure is determined before application of the payload. The only external load is the lifting force. The second case involves a structure loaded with concentrated force applied in the middle of the span. The amount of applied force is limited to the value at which there is no inflection point of deformed line of the substitute elastic rod. In the third case, the structure subjected to concentrated force applied in the middle of the span was analyzed, without limiting the occurrence of inflection points.

#### 3.1 Self-erection state

The first stage of the analysis included only initial stage – self-erection of bending active structure. This is a problem of the initial form of the structure depending on its mechanical properties and the applied lifting force. No cases of the external load were considered at this stage.

A substitute beam-like structure has a roller support *A* and a simple support *B*. The end at the roller support is attached to a cable, which is pulled horizontally through a hole drilled in the simple support, and, after the beam-like structure has deformed to a maximum height *h*, the pulling cable is clamped at the simple support end.

A free body diagram of the system can be drawn, cutting out the cable, and assuming weight is not a significant force. It shows applied horizontal tension load *T* at the location of the roller support pointing toward the simple support, and the equal and opposite reaction *R<sub>H</sub>* load at the simple support. Vertical reactions at the two supports are neglected, as they have to be equal and opposite, but must be zero because there is no external agent capable of counteracting the resulting couple moment. The free body diagram is shown on Figure 2. Two approaches have been applied to the task formulated in this way. The first one is based on the equation of equilibrium of the Euler column with large deflections, while the second one is based on the solution of the *elastica* problem.

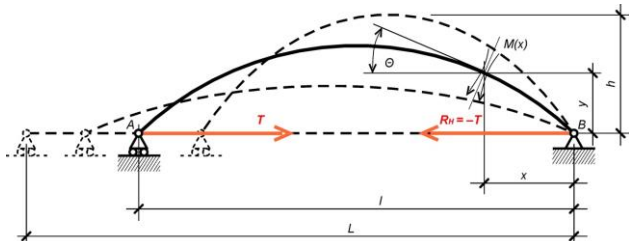


Fig. 2 A free body diagram of modular inflated shell considered as a substitute elastic beam

#### 3.1.1 Formulation based on equation of equilibrium of the Euler column with large deflections

The free body diagram shown on Figure 2 is effectively the same as that of the Euler column. If we make a cut at some coordinate *x* along the length from the simple support *B* to the roller support *A* and take a free-body diagram of one half of the body, the moment equilibrium equation is:

$$M(x) + Ty = 0 \quad (1)$$

Here, *M(x)* is the internal moment, *T* is the tension in the cable, and *y* is the amount of deflection at position *x*. From this point on, further analysis will be carried out in two steps: first, assuming that the deflections are “small enough”, then for large deflections.

#### Solution for small deflection

Assuming a linearly elastic material, the equation (1) for the bending structure can be written as:

$$EI\kappa + Ty = 0 \quad (2)$$

Here, according to Euler-Bernoulli law,  $\kappa$  is the curvature of the elastic curve of the structure:

$$\kappa = \frac{\frac{d^2 y}{dx^2}}{\left[1 + \left(\frac{dy}{dx}\right)^2\right]^{3/2}} \quad (3)$$

If  $\theta$  is introduced as the first derivative of *y*:  $\theta = dy/dx$ , and is then assumed to be an explicit function of *y*, then:

$$\kappa = \frac{\theta \frac{d\theta}{dy}}{\left[1 + \theta^2\right]^{3/2}} \quad (4)$$

When deflections are small, the denominator of the above expression approaches a value of 1 and  $\kappa$  is approximated by the second derivative of *y*.

$$\kappa = \frac{d\theta}{dx} = \frac{d\theta}{dy} \frac{dy}{dx} = \theta \frac{d\theta}{dy} \quad (5)$$

Substituting equation (5) into equation (2) and separating variables yields:

$$\theta d\theta = -\lambda_1^2 y dy \quad (6)$$

Here,  $\lambda_1$  is defined as:

$$\lambda_1 = \sqrt{\frac{T}{EI}} \quad (7)$$

It should be noted that from this point forward that  $\lambda_1$  does not have a strong relationship with *T* as implied by equation (7), but is used simply as a mechanism to derive a compatible shape. The value of *T* is determined through the following methodology.

From the equations (2) and (5) it follows that for “small enough” deflections, moment *M* is related to the second derivative of *y* times *EI*. Given the form of the differential equation, the boundary conditions and the desired result for maximum deflection, a *guess* for the form of *y* is:

$$y(x) = h \sin \frac{\pi x}{\ell} \quad (8)$$

Where, *l* is the current distance between the supports, and is considered an unknown in the problem. The beam-like structure has a net compression transmitted through it; however, at this stage we will ignore the deformation associated with this compression. Thus, for a given value of *h*, the variable *l* can be solved using the equation:

$$L = \int_0^{\ell} \sqrt{1 + \left(\frac{dy}{dx}\right)^2} dx \quad (9)$$

Here, *L* is the length of the beam-like structure when undeformed.

The strain energy of the beam-like structure is formulated by using equations (1) and (8), and on the base of the Clapeyron theorem can be shown to be:

$$U = \frac{T^2 h^2 \ell}{4EI} \quad (10)$$

Applying the Castigliano theorem, one now takes the derivative of the strain energy with respect to *T* to yield the movement of the roller

support toward the simple support, which equals  $L - l$ . Solving for  $T$  yields:

$$T = \frac{2EI}{h^2} \left( \frac{L}{\ell} - 1 \right) \quad (11)$$

Now we can return to equation (6) in order to analyze on this basis the elastic curve of the structure. Integrating equation (6) yields:

$$\frac{1}{2} \theta^2 = -\frac{1}{2} \lambda_1^2 y^2 + C_1 \quad (12)$$

Here,  $C_1$  is an arbitrary constant. Assuming symmetry of deformation and maximum deflection  $h$ , then  $\theta = 0$  when  $y = h$ . Using this boundary condition, solving for  $C_1$  and plugging back into equation (12) yields:

$$\frac{1}{2} \theta^2 = \frac{1}{2} \lambda_1^2 (h^2 - y^2) \quad (13)$$

Manipulating equation (13), remembering the definition of  $\theta$ , and separating variables yields:

$$\frac{dy}{\lambda_1 \sqrt{h^2 - y^2}} = dx \quad (14)$$

Here, we incorporate the boundary condition that when  $x = 0$  then  $y = 0$ . This can be done by taking definite integrals from 0 to  $y$  of the left side of equation (14) and from 0 to  $x$  on the right side of equation (14). It may be advantageous to non-dimensionalize at this point, defining  $\eta$  and  $\xi$  as:

$$\eta = \frac{y}{h}; \quad \xi = \frac{x}{\ell} \quad (15)$$

We then substitute into equation (14) and manipulate to obtain:

$$\frac{d\eta}{\sqrt{1-\eta^2}} = \lambda d\xi \quad (16)$$

Here, the non-dimensional parameter  $\lambda$  is  $\lambda_1$  multiplied by  $l$ . Integrating both sides and rearranging yields:

$$\eta = \sin \lambda \xi \quad (17)$$

When  $\xi = \frac{1}{2}$ ,  $\eta = 1$ ; thus, the simplest assignment for  $\lambda$  is  $\pi$ . Substituting for the non-dimensional variables as defined in equation (15) gives us the half-sine wave shape, which is then used to define the strain energy.

#### Attempt at large deflection solution

Dealing with large deflections is based on a similar approach. Here, the curvature is described by full expression given in equations (3) and (4). The latter term is used on the left-hand side of equation (6) after separation of variables. Following the same procedure as above, and defining  $\beta = h / l$  yields:

$$\frac{\left[ 1 - \frac{1}{2} (\lambda\beta)^2 (1 - \eta^2) \right] d\eta}{\sqrt{1 - \eta^2} \sqrt{1 - \left( \frac{\lambda\beta}{2} \right)^2 (1 - \eta^2)}} \frac{M[(\lambda\beta); \eta]}{\sqrt{1 - \eta^2}} \eta = \lambda d\xi \quad (18)$$

Where  $M$  is a multiplicative factor, which is a function of  $\lambda\beta$  and  $\eta$ :

$$M[(\lambda\beta); \eta] = \frac{1 - \frac{1}{2} (\lambda\beta)^2 (1 - \eta^2)}{\sqrt{1 - \left( \frac{\lambda\beta}{2} \right)^2 (1 - \eta^2)}} \quad (19)$$

It can be seen that for “small” values of  $\beta$  that the left-hand side of equation (18) reduces to that of equation (16).

A few comments should be made about the multiplicative factor  $M$ . First, looking at the square root in the denominator, it is seen that  $\lambda\beta$  can never exceed 2. Looking at the numerator, it is seen that if  $\lambda\beta$  exceeds  $\sqrt{2}$  that negative contributions will be made to the integral. Physically, this implies that the shape of the structure will “double back” in the  $x$  coordinate.

#### Discussion of the results

In order to clarify the meaning of the relations expressed by equation (18), calculations were carried out to allow presentation of particular quantities versus  $\lambda\beta$ . Equation (18) was solved using Simpson’s Rule ) plots are not presented due to the size of the text). Noteworthy is that  $M$  is essentially 1 for  $\eta = 1$ . Also, for  $\lambda\beta = 0$  that  $\lambda = \pi$  as expected. The value of  $\lambda$  then decreases as the non-linearity increases. It should be noted that somewhere between  $\lambda\beta = 1.8$  and 1.9 that  $\lambda$  will go to 0. The physical meaning of this, and the effect on  $\beta$  are not known at this stage of research.

In the next step, the dependence of the deformed curve from  $\lambda\beta$  was determined

$$\int ds = \int \sqrt{(dx)^2 + (dy)^2} = L \quad (20)$$

$$\int d\sigma = \int \sqrt{(d\xi)^2 + (\beta d\eta)^2} = \frac{1}{\gamma} \quad (21)$$

where  $\gamma = l / L$  and  $d\sigma = ds / l$ .

It can be shown that for *small* values of  $\lambda\beta$  that:

$$\gamma \approx 1 - \left( \frac{\lambda\beta}{2} \right)^2 \quad (22)$$

The integration of equation (18) is now used to generate  $\eta$  vs.  $\xi$  plots for selected values of  $\lambda\beta$ . In order to increase the physical meaning of these plots they are converted back to  $y$  and  $x$ , respectively, each non-dimensionalized by  $L$ , by multiplying  $\eta$  by  $\gamma\beta$  and  $\xi$  by  $\gamma$ . These plots are displayed in Figure 3. It is important to note that the full shape of each curve includes a symmetrical segment about the right end of the curve as shown. It should also be noted that for  $\lambda\beta$  approaching 0 the shape is a half sine wave (including the reflected portion of the curve) with infinitesimal height.

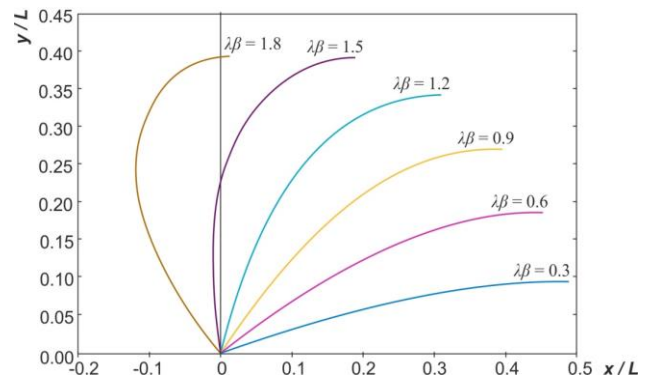


Fig. 3 Shape curves for different values of  $\lambda\beta$

Then, calculations were made to determine the tension  $T$  required to form the shapes noted. As discussed previously, the tension can be determined by taking the derivative of the strain energy with respect to  $T$ . It can be shown that it is related to the shortening of the distance between the two supports by:

$$L - \ell = \frac{T}{EI} \int y^2 ds \quad (23)$$

Note that the integral is taken over the length of the structure, not just the  $x$  coordinate, to account for the large deformation. Non-dimensionalizing and re-arranging yields:

$$\tau = \frac{1}{2\mu(\gamma\beta)^2} \left[ \frac{1}{\gamma} - 1 \right] \quad (24)$$

Here,  $\tau$  represents non-dimensionalized tension defined as  $TL^2 / EI$ , and  $\mu$  represents non-dimensional strain energy:

$$\mu = \int_0^{0.5} \eta^2 d\sigma \quad (25)$$

Of interest is the limit of  $\tau$  as the non-linearity gets small. It should be noted that:

$$\mu = \int_0^{0.5} \sin^2 \pi \xi d\xi = 0.25 \quad (26)$$

Furthermore, if one substitutes the approximation of equation (22), the zero  $\beta$  terms cancel and:

$$\tau = \frac{\lambda^2}{8\mu\gamma^2} = \frac{\pi^2}{2} \quad (27)$$

This appears consistent with the rest of Figure 4. It should be noted that this is half of the classical Euler load for the structure. Figure 4 presents plots of  $\mu$  and  $\tau$ , respectively, vs.  $\lambda\beta$ .

### 3.1.2 Formulation based on the classic problem of the *elastica*

In the second approach the classical problem of the *elastica* has been applied to describe the structural characteristics of inflatable cushion structures, including a proposed method to determine the bending stiffness of these structures. Approximate solutions employing a combination of the *elastica* formulation and the principle of minimum potential energy have been obtained to provide simple expressions for engineers to use to determine the key parameters of the shape in terms of the end rotation.

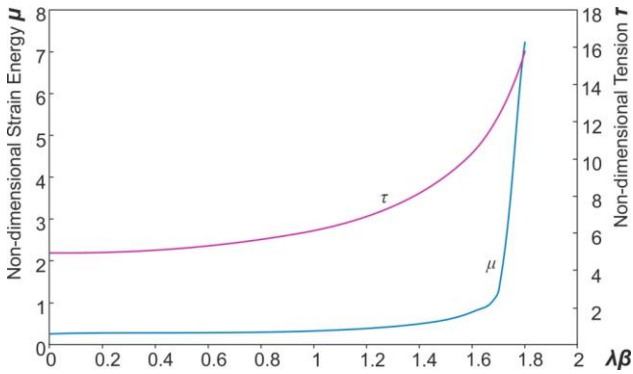


Fig. 4 Non-dimensional strain energy  $\mu$  and non-dimensionalized tension  $\tau$  as a function of the  $\lambda\beta$

Figure 1 displays the inflatable cushion structure in a series of deformed conditions. The figure also displays the key geometric parameters and, for one of the deformed conditions, a free body diagram. Following Ref. 6, the free body diagram indicates that at a coordinate  $x$  along the horizontal analysis, or, preferably, a coordinate  $s$  along the (assumed fixed) length of the structure, the equilibrium equation is given by Eq. (1). The equivalency to the *elastica* problem is now demonstrated. The following relationships will be used in the derivation:

$$\frac{dy}{ds} = \sin \theta \quad (28a)$$

$$\frac{dx}{ds} = \cos \theta \quad (28b)$$

$$M = EI\kappa \quad (28c)$$

$$\kappa = \frac{d\theta}{ds} \quad (28d)$$

Taking a derivative of Eq. (1) with respect to  $s$ , multiplying the equation by the curvature  $\kappa$  and substituting several of the relations of Eq. (28) yields:

$$EI \frac{d^2\theta}{ds^2} \frac{d\theta}{ds} + T \sin \theta \frac{d\theta}{ds} = 0 \quad (29)$$

This expression is equivalent to:

$$\frac{d}{ds} \left[ \frac{1}{2} EI \left( \frac{d\theta}{ds} \right)^2 - T \cos \theta \right] = 0 \quad (30)$$

The expression in the brackets of Eq. (30) is thus constant along the arc length of the structure. Essentially, this is the *elastica* problem of Love (Ref. 11).

The value of the constant is determined from the boundary conditions. If the value of  $\theta$  when  $s = 0$  is specified as  $\theta_0$ , and noting that the curvature is zero at that point, yields:

$$\frac{1}{2} EI \left( \frac{d\theta}{ds} \right)^2 = T(\cos \theta - \cos \theta_0) \quad (31)$$

The solution for  $\theta(s)$  is found in Love (Ref. 11) using a change in variable and “elliptical functions of the second kind”. These functions are not familiar to most engineers. Accordingly, a numerical solution to Eq. (31) will be employed. Later in this paper, approximate analytical methods will be used to lend analytical meaning to the results, particularly when  $\theta_0$  is small.

Separating variables in Eq. (31) yields the following intrinsic solution for  $\theta(s)$ :

$$\int_{\theta_0}^{\theta} \frac{d\theta}{\sqrt{2(\cos \theta - \cos \theta_0)}} = \frac{\pi}{L} \sqrt{\frac{T}{P_E}} s \quad (32)$$

Here,  $P_E$  is the classical Euler buckling load the structure.

The numerical procedure is as follows: for a given value of  $\theta_0$ , the integral on the left side of Eq. (32) is evaluated for different values of  $\theta$  from  $\theta_0$  to 0, generating  $\theta(s)$  in tabular form. At  $\theta = 0$ ,  $s = L/2$ . This then solves for  $T/P_E$  as a function of  $\theta_0$ .

The integrand on the left hand side of Eq. (32) is singular at the beginning of the integration range. In order to start the integral process (generally done with Simpson’s rule), a small step of size  $\varepsilon_0$  is chosen. Let  $\varepsilon$  be a value of  $\theta$  between  $\theta_0$  and  $\theta_0 - \varepsilon_0$ ; then, the integrand is approximately:

$$\frac{d\theta}{\sqrt{2(\cos \theta - \cos \theta_0)}} = \frac{d\varepsilon}{\sqrt{2\varepsilon \sin \theta_0}} \quad (33)$$

Integrating from 0 to  $\varepsilon_0$ , and noting that for the computations used  $\varepsilon_0 = 2 \times 10^{-6} \theta_0$ , the initial step is thus  $0.002 \sqrt{\theta_0 / \sin \theta_0}$ .

In order to plot the deformed shape of the structure, the  $x$  and  $y$  coordinates are found parametrically as functions of  $s$  by integrating Eqs. (28a) and (28b) respectively. The deformed span  $\ell$  is found by integrating Eq. (28a) from 0 to  $L$ , while the maximum height  $h$  is found by integrating Eq. (28b) from 0 to  $L/2$ .

Figure 5 displays the various shapes of the structure for different values of  $\theta_0$ . Note that half the shape is shown. The rest of the shape is symmetric about the end opposite the end at the origin.

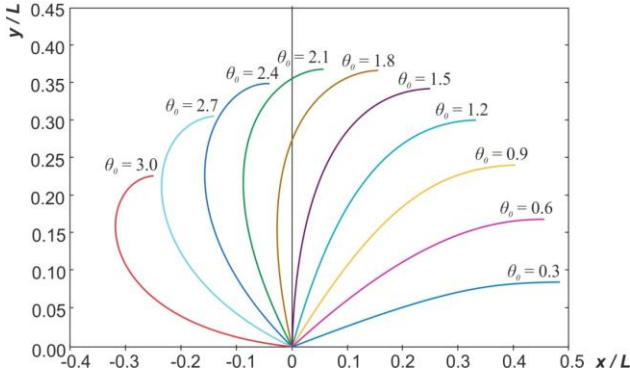


Fig. 5 Derived shapes for the structure as a function of  $\theta_0$

Note that for values of  $\theta_0$  greater than about 2.3 radians the structure deforms into a loop. While mathematically interesting, it is not physically possible with the inflatable cushion system. The blue curve of Figure 6 displays the maximum height of the structure as a function of  $\theta_0$ . Note that the tallest structure occurs when  $\theta_0$  is about 2.0 radians, where  $h/L$  is slightly more than 0.4.

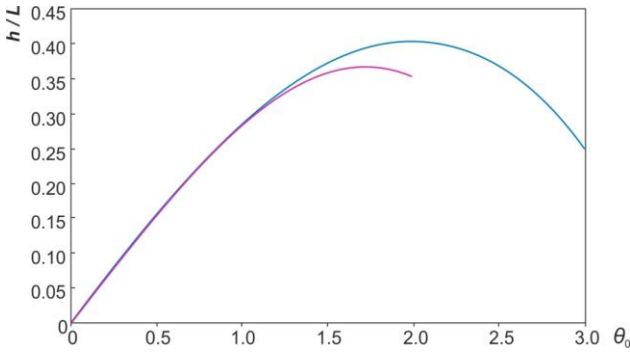


Fig. 6 Maximum height of the structure as a function of  $\theta_0$

The blue curve of Figure 7 displays the tension in the attached cable required to hold the structure in a particular deformed shape as a function of  $\theta_0$ .

Note that as  $\theta_0$  goes to 0 that the problem reduces to the classical Euler buckling problem. Approximating the cosines by the first two terms of their Taylor series yields in the left-hand side of Eq. (6) yields:

$$\int_{\theta_0}^0 \frac{d\theta}{\sqrt{2(\cos\theta - \cos\theta_0)}} = \int_{\theta_0}^0 \frac{d\theta}{\sqrt{\theta_0^2 - \theta^2}} = \cos^{-1} \frac{\theta}{\theta_0} \Big|_{\theta_0}^0 = \frac{\pi}{2} \quad (34)$$

Setting this to the right hand side of Eq. (32) with  $s = L/2$  yields  $T = P_E$ .

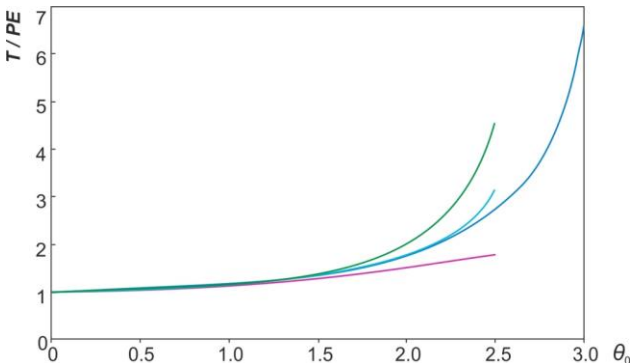


Fig. 7 Required tension as a function of  $\theta_0$

### Comparison with experiment

In Refs 2-4, the author did experimental research with inflatable cushion structures similar to those described herein. In one case, the pull cable

was loaded so that the horizontal expanse of the structure was 50% of the structure length. Referring to Eq. (28a) and remarks above, this situation would occur when  $\theta_0$  is about 1.5 radians, or slightly less than  $90^\circ$ . In fact, this is nearly the case. Proceeding with this result yields that the maximum height, as determined from Figure 6, is about  $3/8$  of the length of the structure. This, too, is not significantly different from the experimental result. Finally, the required tension to hold this shape is determined from Figure 7 and is seen to be about  $1.35 P_E$ . Thus the bending stiffness is experimentally determined to be:

$$EI = \frac{TL^2}{1.35\pi^2} = 0.075TL^2 \quad (35)$$

### Approximate analytical solutions

In order to lend greater physical meaning to the results, approximate analytical solutions are sought for the quantities plotted in Figures 6 and 7. These approximations will be for small values of  $\theta_0$ . Using Eq. (34) but with variable upper limit as a guide:

$$\theta(s) \approx \theta_0 \cos \frac{\pi s}{L} \quad (36)$$

In order to find the horizontal expanse of the deformed structure, Eq. (28b) is integrated over the range of  $s$ ; thus:

$$\ell = \int_0^L \cos \theta ds \approx \int_0^L \left[ 1 - \frac{1}{2} \theta^2 \right] ds \quad (37)$$

Substituting Eq. (36) into Eq. (37) yields:

$$\ell/L = 1 - \frac{\theta_0^2}{4} \quad (38)$$

Note that in this approximate expression there is excellent agreement with the "exact" solution for  $\theta_0 < 1$  radian.

In order to find the maximum height of the deformed structure, Eq. (28a) is integrated over the half-range of  $s$ ; thus:

$$h = \int_0^{L/2} \sin \theta ds \approx \int_0^{L/2} \left[ \theta - \frac{\theta^3}{6} \right] ds \quad (39)$$

Substituting Eq. (36) into Eq. (39) yields:

$$h/L = \frac{1}{\pi} \left( \theta_0 - \frac{\theta_0^3}{9} \right) \quad (40)$$

The approximate expression is plotted in magenta in Figure 6. Note that here as well there is excellent agreement with the "exact" solution for  $\theta_0 < 1$  radian.

In order to find an approximate expression for the required tension for a particular shape, some manipulation must be carried out on the equilibrium equation in order to derive a criteria for determining  $T$ . Multiplying Eq. (1) by the variation of the curvature, integrating over the range of  $s$ , and substituting Eqs. (28c) and (28d) yields:

$$\int_0^L \left[ EI \kappa \delta \kappa + Ty \delta \left( \frac{d\theta}{ds} \right) \right] ds = 0 \quad (41)$$

Integrating the second term in the integrand by parts and substituting Eq. (28a) yields:

$$\int_0^L \left[ EI \kappa \delta \kappa - T \sin \theta \delta \theta \right] ds + Ty \delta \theta \Big|_0^L = 0 \quad (42)$$

The last term is zero because  $y = 0$  at either end of the structure. Note that Eq. (42) can be manipulated to yield:

$$\delta \left( \int_0^L \left[ \frac{1}{2} EI \kappa^2 - T(1 - \cos \theta) \right] ds \right) = 0 \quad (43)$$

The first term, when integrated, is the strain energy  $U$ . The second term can also be integrated to yield:

$$\delta(U - T(L - \ell)) = 0 \quad (44)$$

Eq. (44) is recognized as the principle of minimum potential energy for the inflated cushion structure. Employing Eq. (44) (or its form in Eq. (43)) and using Eq. (36) to approximate  $\theta$  will yield an approximate expression for the tension  $T$ .

The potential energy, denoted by  $\Pi$ , can first be approximated as:

$$\Pi \approx \int_0^L \left[ \frac{1}{2} EI \left( \frac{d\theta}{ds} \right)^2 - T \left( \frac{\theta^2}{2} - \frac{\theta^4}{24} \right) \right] ds \quad (45)$$

Substituting Eq. (36) and integrating yields:

$$\Pi = \frac{L}{4} \left[ P_E \theta_0^2 - T \left( \theta_0^2 - \frac{\theta_0^4}{16} \right) \right] \quad (46)$$

Taking a derivative of  $\Pi$  with respect to  $\theta_0$  and setting to zero yields:

$$\frac{T}{P_E} = \frac{1}{1 - \frac{\theta_0^2}{8}} \quad (47)$$

This approximate expression is plotted in Figure 7 in green. This expression is in excellent agreement with the "exact" solution for  $\theta_0 < 1$  radian. Eq. (47) can be further approximated as:

$$\frac{T}{P_E} = 1 + \frac{\theta_0^2}{8} \quad (48)$$

This expression is plotted in Figure 7 in magenta and also is fairly accurate for  $\theta_0 < 1$  radian. Finally, the average of the expressions in Eqs. (47) and (48) are plotted in Figure 7 in cyan. Note that this expression is in agreement with the "exact" solution for  $\theta_0 < 2.2$  radians. This limit is well within any practical applications for inflatable cushion structures.

### 3.2 Shell under applied transverse loading

#### 3.2.1 Extension of the *elastica* problem to the problem of inflated cushions under transverse loading.

To formulate a computational model of a modular inflatable cushion structure under applied transverse loading, the free body diagram shown in Figure 2 has been modified in accordance with Figure 8. The structure is under a general vertical load distribution  $w$ , which is assumed known and can be expressed as function of  $s$ , the coordinate along the (assumed fixed) length of the structure.

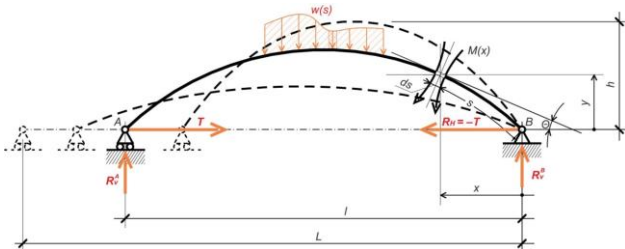


Fig. 8 Computational model

In Ref. 7, the potential energy expression for the *elastica* problem (that is, the problem herein with  $w = 0$  over the entire length of the structure) was derived. This expression is:

$$\Pi = U - T(L - \ell) \quad (49)$$

Here,  $U$  is the strain energy. The second term subtracted is the work done by the tension in the draw rope.

The expression is extended for two effects. The first is the work done by the applied load  $w$  through the vertical deflection  $y$ . This term introduces a second displacement variable  $y$  in addition to the variable  $\theta$  used in Ref. 7 and 11. Accordingly, a Lagrange multiplier, which is also a function of  $s$ , is introduced, multiplying the geometric relationship between  $y$  and  $\theta$ . The resulting expression for the potential energy is thus:

$$\Pi = \int_0^L \left[ \frac{1}{2} EI \left( \frac{d\theta}{ds} \right)^2 - T(1 - \cos \theta) + wy + V \left( \frac{dy}{ds} - \sin \theta \right) \right] ds \quad (50)$$

Here,  $EI$  is the bending stiffness, the horizontal span change is expressed as an integral and the Lagrange multiplier is designated as  $V$ . The choice of this symbol for the Lagrange multiplier will become apparent as the formulation progresses.

Minimizing the potential energy using calculus of variations yields the following three equations for the three variables  $\theta$ ,  $y$  and  $V$ :

$$\begin{aligned} EI \left( \frac{d^2\theta}{ds^2} \right) + T \sin \theta + V \cos \theta &= 0 \\ \frac{dV}{ds} - w &= 0 \\ \frac{dy}{ds} - \sin \theta &= 0 \end{aligned} \quad (51)$$

The first of these equations is the moment equilibrium equation; the second is the force equilibrium equation in the vertical direction; the third is the geometric relationship between  $y$  and  $\theta$ . Note that  $V$  is thus identified as the upward vertical force transmitted through the structure. To make a comparison with the *elastica* problem the moment equilibrium equation is multiplied by the curvature, that is, the first derivative of  $\theta$  with respect to  $s$ . Initially, this yields:

$$\frac{d}{ds} \left[ \frac{1}{2} EI \left( \frac{d\theta}{ds} \right)^2 - T \cos \theta \right] + V \cos \theta \frac{d\theta}{ds} = 0 \quad (52)$$

The first term, of course, comprises the *elastica* problem. It should be noted that:

$$\frac{d}{ds} (V \sin \theta) = V \cos \theta \frac{d\theta}{ds} + w \sin \theta \quad (53)$$

where use has been made of the force equilibrium equation. Substituting Eq. (53) into Eq. (52) yields:

$$\frac{d}{ds} \left[ \frac{1}{2} EI \left( \frac{d\theta}{ds} \right)^2 - T \cos \theta + V \sin \theta \right] = w \sin \theta \quad (54)$$

Eq. (54), combined with the force equilibrium equation, comprise the extension of the *elastica* problem to the problem of inflated cushions under transverse loading.

#### 3.2.2 Case study 1: a downward point force applied at mid-span

Examining Eq. (54) reveals that the methodology of Gellin and Tarczewski (Ref. 7) would have to be modified when  $w$  is non-zero. In order to use that methodology, a case must be selected that is non-trivial, both analytically and practically, but generally has  $w = 0$ . The case of the downward point force of magnitude  $F$  applied at mid-span is such a case. Note that by symmetry only half the structure need be analyzed; furthermore, the value of  $V$  in one half of the structure is  $-F/2$ , a constant. Figure 9 displays the problem with a free body diagram for the portion of the structure to the right of a cut at a coordinate  $s$  within the right half of the structure.

As a result, Eq. (54) simplifies to:

$$\frac{d}{ds} \left[ \frac{1}{2} EI \left( \frac{d\theta}{ds} \right)^2 - T \cos \theta - \frac{F}{2} \sin \theta \right] = 0 \quad (55)$$

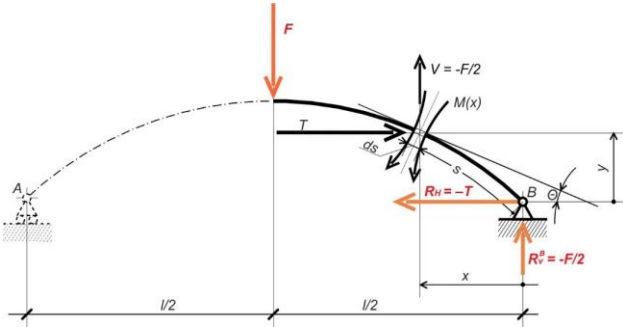


Fig. 9 Free body diagram for the case study

Except for the inclusion of the third term within the brackets, Eq. (55) is in the same form as the *elastica* problem. The bracketed term has a constant value over one-half of the structure. If the value of  $\theta$  at the support at  $s = 0$  is assigned the symbol  $\theta_0$ , then:

$$\frac{1}{2} EI \left( \frac{d\theta}{ds} \right)^2 = T (\cos \theta - \cos \theta_0) - \frac{F}{2} (\sin \theta_0 - \sin \theta) \quad (56)$$

Manipulating Eq. (56) as done in Gellin and Tarczewski [5] yields:

$$\int_{\theta_0}^{\theta} \frac{d\theta}{\sqrt{2 [ \cos \theta - \cos \theta_0 - \beta (\sin \theta_0 - \sin \theta) ]}} = \pi \sqrt{\frac{T}{P_E}} \frac{s}{L} \quad (57)$$

The parameter  $\beta$  is defined as  $F / 2T$ ; the parameter  $P_E$  is the Euler buckling load of the structure. The parameter  $\beta$  is a convenient parameter to generate results. It is related to the applied load, but not linearly, as it is anticipated that  $T$  will be varying as well with increasing load.

The methodology for Eq. (57) will be the same as that used in Gellin and Tarczewski (Ref. 7): For given values of  $\theta_0$  and  $\beta$  the integral is evaluated for all angles from  $\theta = \theta_0$  to  $\theta = 0$ . At this last point  $s = L / 2$ ; thus, the value of  $T / P_E$  is determined. The integral is then scaled back to determine a  $\theta$  vs.  $s$  table, from which  $x$  and  $y$  coordinates can be generated.

There are some additional conditions of which one should be aware. There is a limitation on  $\beta$  so that the term under the square root sign does not go negative. This will first occur at  $\theta = 0$ , and has a value of:

$$\beta_{\max} = \frac{1 - \cos \theta_0}{\sin \theta_0} \quad (58)$$

The method itself has inherent assumptions built in; in particular, there is an assumption that  $\theta$  does not become negative prior to  $s = L / 2$ . If this did occur, a point of inflection in the shape of the structure would be present. When the curvature reverses, the direction of the moment would reverse. Thus, it is necessary to check the sign of the moment, given by:

$$M = Ty - \frac{F}{2} x \quad (59)$$

where here the moment is considered positive when reacting the tension in the draw rope and thus negative of that shown in Figure 9. (It should be noted that Eq. (55) could be derived from Eq. (59) with the moment defined as in Figure 9.) While it is recognized that such shapes could exist in an equilibrium state, the physical condition of potential ponding when deployed outdoors makes them undesirable.

Finally, the analysis must reflect the physical deployment of the structure. It is imagined that the draw rope will be pulled until the horizontal span of the structure reaches a desired length. The rope would then be clamped into place, fixing this span. As the load is applied, the shape will tend to flatten and bulge, so that it is anticipated that  $\theta_0$  would likely increase. This, in turn, will increase  $\beta_{\max}$ , which will allow larger values of  $\beta$  to be admissible. In the interest of brevity, two cases are considered:  $\ell / L = 0.50$  and  $0.75$ . A range of values of  $\beta$  beginning with zero will be studied until one of the conditions of the analysis is violated.

The results are presented in the following figures. Figure 10 indicates how the values of  $\beta$  and  $\beta_{\max}$  converge before a contradiction in the methodology occurs.

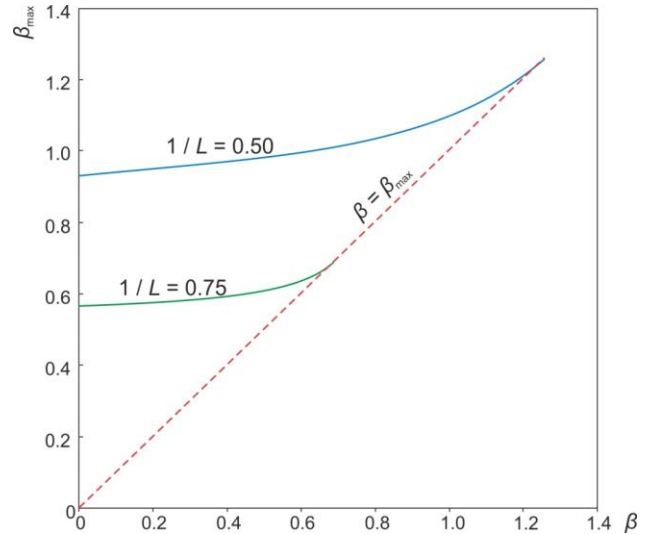


Fig. 10 Variation of  $\beta_{\max}$  with  $\beta$

Figures 11(a) and 11(b) display the derived shapes of the structure as the load increases, up to the limiting value of  $\beta$  given in Figure 10. As is seen in the figures, the shapes bulge as the load increases.

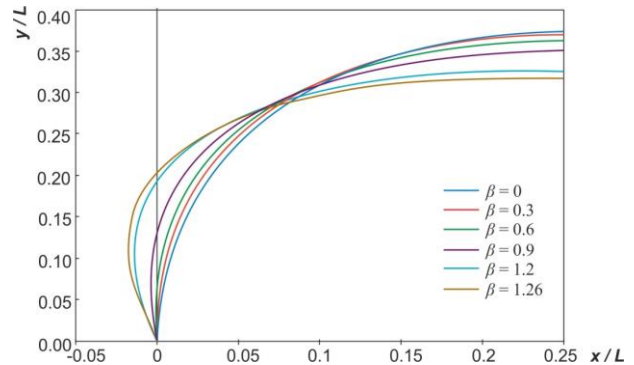


Fig. 11(a) Half shape for  $\ell / L = 0.50$

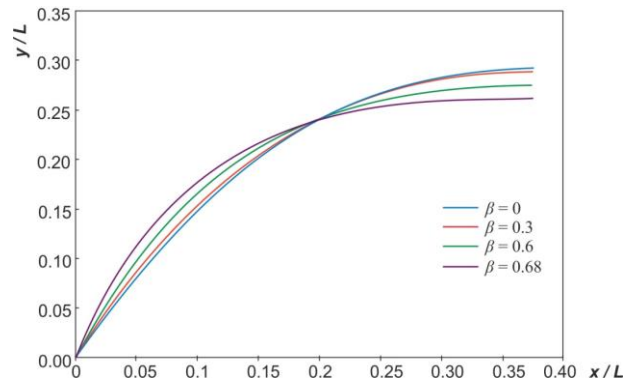


Fig. 11(b) Half-shape for  $\ell / L = 0.75$

Figure 12 displays how the tension in the draw-rope increases with increasing load. It is seen that the tension increases more rapidly if the initial span is longer and flatter.

Figure 13 displays the variation in the bending moment with increasing load. Of interest are the maximum moment and the moment at the mid-span. When  $\beta = 0$  (the *elastica*), the maximum bending moment exists at the mid-span. As the load increases, the maximum moment moves toward the interior of the half-span; the moment at the mid-span steadily decreases until it goes negative, indicating that the methodology is no longer valid. It is interesting to note that the maximum moment actually decreases initially with increasing load before increasing with increasing applied load.

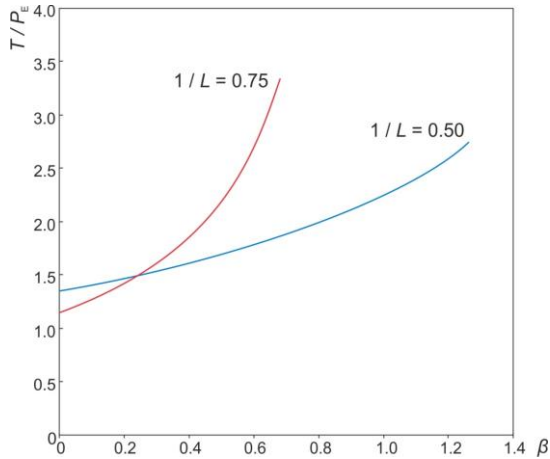


Fig. 12 Variation of the draw-rope tension with increasing load

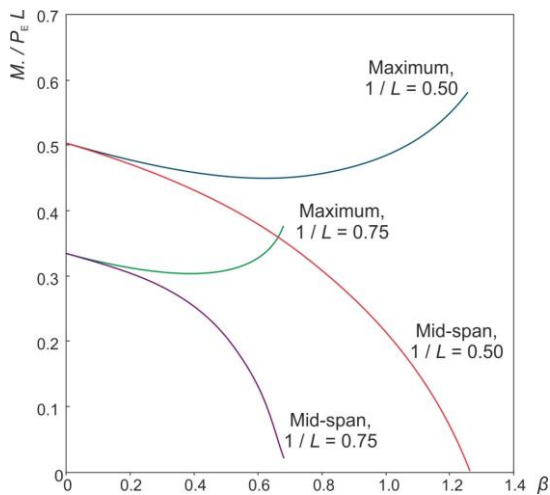


Fig. 13 Moment variation with increasing load

Figure 14 displays the applied force as a function of  $\beta$ . It is a true measure of the strength of the inflated cushion structure. Note that the shorter horizontal span case has the potential to carry more load.

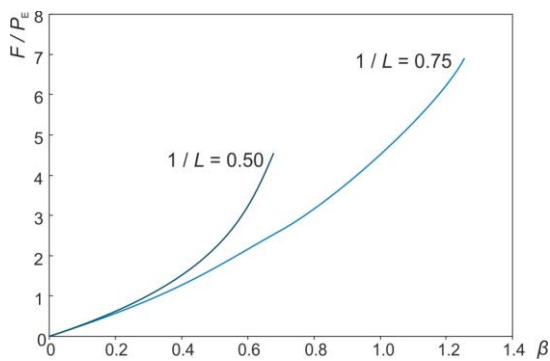


Fig. 14 Applied load as a function of  $\beta$

### 3.2.3 Case study 2: a downward point force applied at mid-span with inflection points

In this chapter, the authors successfully use an alternate method of solution which allows for inflection points to be included in the derived shapes. This allows for study of these structures under increased load. Results for those cases examined above in chapter 3.2.2 using the current methodology are in agreement with the results derived below.

The equation of moment equilibrium was derived above in chapter 3.2.2, Eq. (55). This equation was subsequently manipulated to obtain Eq. (57). There,  $P_E$  is the Euler buckling load of the structure and  $\theta_0$  is the angle of rotation of the structure at the support. The method of solution uses the parameter  $\beta = F / 2T$  as the basic parameter for study with a particular span  $\ell / L$ . A value of  $\theta_0$  is then chosen. The integral in Eq. (57) is then calculated for all values from  $\theta_0$  to 0. The value of  $s$  when  $\theta = 0$  is  $L / 2$ . Thus, the ratio  $T / P_E$  is calculated as well as all the other parameters of the problem. Most importantly, a value of  $\ell / L$  is calculated. If it is not the particular span under study then the value of  $\theta_0$  is changed and the process is repeated until convergence.

The method works well for cases where the ratio  $F / 2T$  is below a certain threshold determined by a non-negative bending moment at mid-span. Only one parameter,  $\theta_0$ , is varied in order to obtain a complete solution. However, the algorithm has short-comings. First, the form of Eq. (57) is such that one is actually calculating  $s$  as a function of  $\theta$  rather than the other way around. This implies that  $\theta$  should be single valued and, given the boundary condition, non-negative. It appears that this is geometrically restrictive on the geometry of the deformed structure, as well as the fact that there appears to be no physical reason for this restriction to occur. Secondly, the presence of the square root implies an additional restriction between the parameter  $F / 2T$  and  $\theta_0$ . Finally, it is anticipated that  $T$  increases with increasing  $F$ , and thus it is unknown if a limit on the ratio  $F / 2T$  may exist. The parameter itself appears to be arbitrarily chosen, but it does allow for an independent assessment of value of  $T / P_E$ .

Accordingly, a modification of the method of solution was developed. It is based on Eq. (55). Defining the non-dimensional variable  $\zeta$  as  $s / L$ , Equation (55) transforms to:

$$\frac{d^2\theta}{d\zeta^2} + \pi^2 \left( \frac{T}{P_E} \sin\theta - \frac{F}{2P_E} \cos\theta \right) = 0 \quad (60)$$

The boundary conditions are:

$$\frac{d\theta}{d\zeta}(0) = 0; \theta\left(\frac{1}{2}\right) = 0 \quad (61)$$

Equation (60) is solved by a central difference method. The advantages of this method are that  $\theta$  is found as a function of  $\zeta$ , which is a naturally single-valued variable. Thus,  $\theta$  can decrease and increase as needed. The parameter for study is  $F / P_E$ , which is a natural parameter to represent the applied load. The disadvantages are that the central difference method is usually employed with initial value problems. In this case, a particular value of  $\theta_0$  is assumed. Furthermore, unlike the method of [6], a value of  $T / P_E$  is also assumed. These values are changed at each iteration until the span value  $\ell / L$  and the second boundary condition of Eq. (61) are satisfied. It was found that as  $F / P_E$  increases, the ability to converge to a satisfactory condition became more difficult. The results below perhaps offer a clue as to possible reasons.

### Results

As in chapter 3.2.2, two main case studies are considered,  $\ell / L = 0.50$  and  $\ell / L = 0.75$ . The derived shapes are displayed in Figure 15, below.

For the first case, inflection points in the half-shape are clearly present as  $F / P_E$  increases, beginning with a value of 8 for that parameter. Similarly, for the second case, inflection points begin when this force parameter is about 5. This corresponds to the results of chapter 3.2.2, where the maximum values of the  $F / P_E$  parameter for shapes without inflection points were about 7 and 4.5 respectively for the two spans studied.

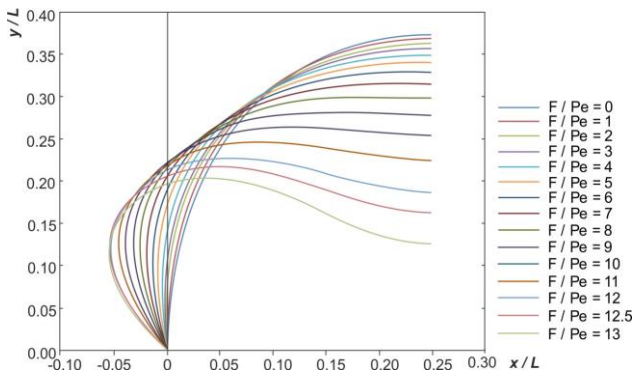


Fig. 15(a) Half shape for  $\ell / L = 0.50$

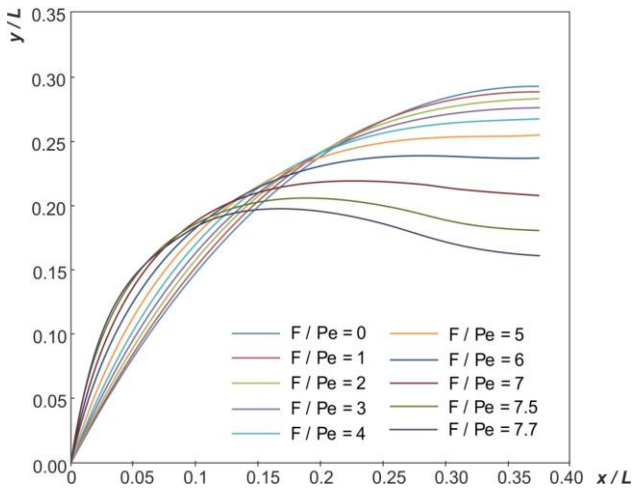


Fig. 15(b) Half-shape for  $\ell / L = 0.75$

Figure 16 displays the tension in the pull rope as a function of the applied load. Note the increasing rate of increase of this parameter as the load on the structure increases. For both span cases the curves are becoming vertical at the maximum loads studied.

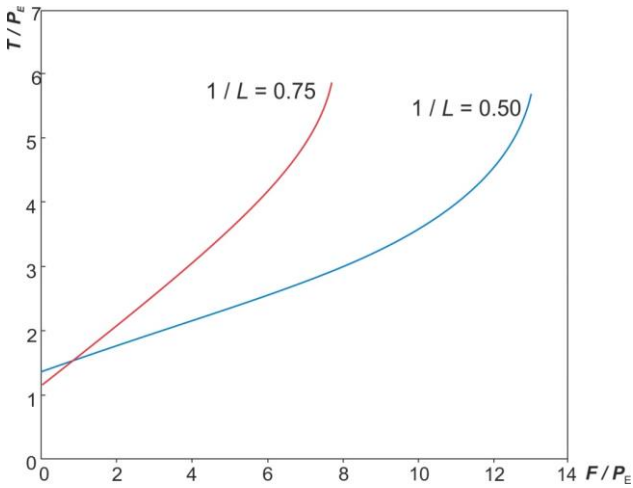


Fig. 16 Tension in the draw rope

Figure 17 displays the bending moment at mid-span ( $M_c$ ) and the maximum bending moment in the half-span ( $M_{max}$ ) of the inflated cushion structure. A negative mid-span bending moment is indicative of the presence of inflection points in the interior of the half-span shape.

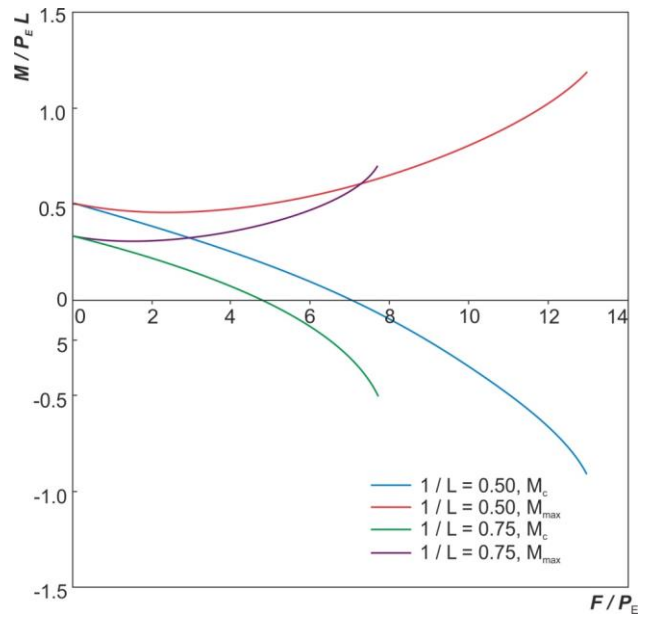


Fig. 17 Bending moments

Figure 18 displays the mid-span stiffness of the structure normalized by the mid-span bending stiffness of a simply supported beam,  $k_0 = 48 EI / L^3$ . It is seen that the inflated cushion structure, modeled as an active bending member, is significantly stiffer than a straight flat beam. This agrees qualitatively with the results of Ref. 12. Note that as the magnitude of the applied force increases that the stiffness decreases.

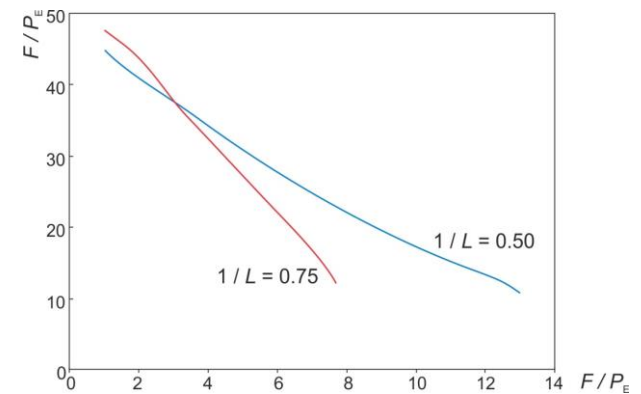


Fig. 18 Mid-span stiffness

To explain the difficulty in achieving convergence with loads larger than those shown, one returns to Figures 16 and 18. It appears that the tension in the rope to maintain the deployed structure at a particular span length is increasing very rapidly. This may lead to failure of the rope or compressive failure of the structure; furthermore, the rapidly decreasing stiffness will result in the mid-span hitting the ground or falling below the level of the supports, or some sort of “snap-through” buckling phenomenon resulting in a loss of load carrying capacity. To illustrate the course of the process, comparison of shapes of the inflated cushion structure after uplift to  $\ell / L = 0.50$ , for different values of  $F / P_E$ , are shown in Figure 19. Regardless, the study shows some practical limitations for the effectiveness of these structures.

#### 4. CONCLUDING REMARKS

A methodology for studying the behavior of inflated cushion structures modeled as an active bending member has been derived. Shapes including inflection points have been derived and appear to be stable. It

appears a limitation on the point load is possible based on rapidly increasing tension in the draw rope and decreasing stiffness of the structure with increasing load. Future work will attempt to use this methodology to study more complex load cases, such as weight and, to a lesser extent, snow loads.

In parallel with the work on analytical solutions, work is underway on a computational model of the structure being studied using FEM. The model being developed will take into account the details of the construction of the real structure, in particular the possibility of the cable sliding relative to cross-braces in the nodes of the lower chord.

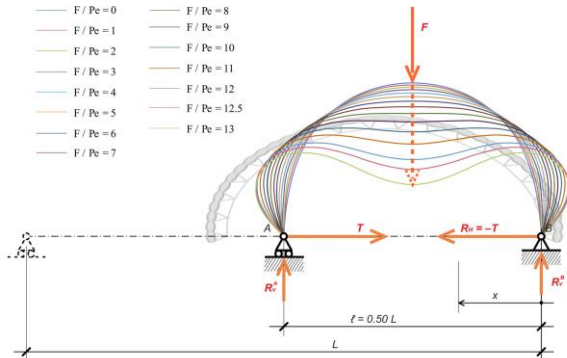


Fig. 19 Comparison of shapes of the inflated cushion structure after uplift to  $l/L = 0.50$ , for different values of  $F/P_E$

#### ACKNOWLEDGEMENTS

The first author would like to thank Birdair, Inc. and its parent company Taiyo-Kogyo Corporation for support of this work.

#### REFERENCES

1. Tarczewski R., "Self-erecting pneumatic structures", *Mobile and Rapidly Assembled Structures*, F. ESCRIG and C.A. BREBBIA (Eds.), Boston, 2000
2. Tarczewski R., "Post-tensioned modular inflated structures. *Computational Methods in Applied Sciences*, 2005; **3**: 221-239.
3. Tarczewski R., "Physical modeling of modular inflated shells – an initial research", in *Lightweight Structures in Civil Engineering*, J.B. OBRĘBSKI (Ed.), Warszawa, 2005
4. Tarczewski R. *et al.*, "Improvement of the system of modular inflated shells by means of physical modeling", *Structural Membranes – Textile Composites and Inflatable Structures VI*, E. Oñate, K.-U. Bletzinger and B. Kröplin (Eds.), Barcelona, 2011
5. Gellin S. and Tarczewski R., "Modular inflated shells – a computational approach", *Structural Membranes – Textile Composites and Inflatable Structures VII*, E. Oñate, K.-U. Bletzinger and B. Kröplin (Eds.), Barcelona, 2015
6. Gellin S. and Tarczewski R., "Computational modeling of bending active modular inflated structures", *IASS 2015. Future Visions*, J. Coenders (Ed.), Amsterdam, 2015
7. Gellin S. and Tarczewski R., "Inflatable cushions, active bending and the elastica", in *IASS 2016, Spatial Structures in the 21st Century* K. Kawaguchi, M. Ohsaki and T. Takeuchi (Eds.), Tokyo, 2016
8. Gellin S. and Tarczewski R., "Extension of elastica methodology to inflated cushions under applied transverse loading," *IASS 2017, Interfaces: architecture, engineering, science*, A. Bogle and M. Grohmann (Eds.), Hamburg, 2017
9. Gellin S. and Tarczewski R., "Point force on inflated cushions with inflection points", *IASS 2018, Creativity in Structural Design*, C. Mueller and S. Adriaenssens (Eds.), Boston, Boston, 2018
10. Gellin S. and Tarczewski R., "Inflated cushions under uniformly distributed loading", *Structural Membranes – Textile Composites and Inflatable Structures IX*, E. Oñate, K.-U. Bletzinger and B. Kröplin (Eds.), Barcelona, 2019 (to appear)
11. Love, A.E.H., *A Treatise on the Mathematical Theory of Elasticity*. (4<sup>th</sup> ed.), Dover, 1944.
12. C. Lazaro, S. Monleon and J. Bessini, "Tangent stiffness in point-loaded elastica arches," in *IASS 2017, Interfaces: architecture, engineering, science, Hamburg, September 25 – 28, 2017*, A. Bogle and M. Grohmann Eds., 2017